Mohammad F. Hadi
Department of Biomedical Engineering,
University of Minnesota,
7-105 Hasselmo Hall, 312 Church Street SE,
Minneapolis, MN 55455
e-mail: hadix004@umn.edu

Edward A. Sander
Department of Biomedical Engineering,
University of Iowa,
1402 Seamans Center,
Iowa City, IA 52242
e-mail: edward-sander@uiowa.edu

Victor H. Barocas[1]
Department of Biomedical Engineering,
University of Minnesota,
7-105 Hasselmo Hall, 312 Church Street SE,
Minneapolis, MN 55455
e-mail: baroc001@umn.edu

Multiscale Model Predicts Tissue-Level Failure From Collagen Fiber-Level Damage

Excessive tissue-level forces communicated to the microstructure and extracellular matrix of soft tissues can lead to damage and failure through poorly understood physical processes that are multiscale in nature. In this work, we propose a multiscale mechanical model for the failure of collagenous soft tissues that incorporates spatial heterogeneity in the microstructure and links the failure of discrete collagen fibers to the material response of the tissue. The model, which is based on experimental failure data derived from different collagen gel geometries, was able to predict the mechanical response and failure of type I collagen gels, and it demonstrated that a fiber-based rule (at the micrometer scale) for discrete failure can strongly shape the macroscale failure response of the gel (at the millimeter scale). The model may be a useful tool in predicting the macroscale failure conditions for soft tissues and engineered tissue analogs. In addition, the multiscale model provides a framework for the study of failure in complex fiber-based mechanical systems in general. [DOI: 10.1115/1.4007097]

Keywords: multiscale modeling, tissue failure, biomechanics, collagen, biomaterials

1 Introduction

Extracellular matrix proteins are assembled into complex hierarchical structures in a tissue-specific manner to provide tissue stability and to enable tissue function. When tissue-level forces exceed the physiological range, ECM components can be damaged, the stability of the tissue can become compromised, and the tissue can become nonfunctional. For example, in whiplash injuries, where abnormal head and neck kinematics produce excessive cervical facet deformation, painful microtears may develop in the cervical facet capsular ligament [1]. Alternatively, pathological remodeling can lead to alterations in the tissue microstructure that progressively weaken it and make it susceptible to catastrophic failure. Such is the case with aortic aneurysms, where the stress in the aortic wall exceeds the local tissue strength, and the vessel ruptures or dissects, often with fatal consequences [2]. In both cases, there is a fundamental lack of understanding of how tissue-level loads are communicated to the ECM microstructure and lead to tissue damage and failure. Because of the lack of understanding of multiscale failure phenomena, the biomedical community is limited in its ability to prevent, diagnose, and treat soft tissue injuries and diseases of this nature.

To understand tissue failure better, several important models have been developed that incorporate aspects of the tissue microstructure, often through collagen fiber crimp, fiber orientation, and strain-based recruitment and failure distributions [3–6]. Although these models can describe failure phenomena, they are constrained in their ability to provide insight into the mechanisms of failure because the description of the tissue microstructure is limited or essential elements such as fiber-fiber interactions and realistic fiber kinematics are absent. Others have focused on the importance of these elements as they relate to lung [7], intermediate filaments in the cytoskeleton [8,9], and nonbiological materials [10,11], but those models are either two-dimensional or limited to the behavior of a single network. Zohdi [12] has successfully modeled multiscale failure in regular lattices of biological fibers, and Ernst et al. [13] have also explored multiscale fiber network failure (though in a nonbiological context) using a regular unit cell with periodic boundaries. Most tissues are much more complex and display regional inhomogeneities in microstructure, fiber organization, and mechanical properties, such that the mechanical response of the tissue derives from the integrated deformation and distribution of load throughout the tissue ECM. Hence, for these types of tissues, any model predicated on mechanisms of local fiber failure must contain an explicit three-dimensional description of the ECM microstructure and the spatial heterogeneity of the tissue. Recent studies support the need for this level of detail, as they report nonaffine fiber reorganization [14–16] and regional variations in the mechanical behavior in response to load [17,18], including an example of complex relationships between the noncoincident locations of damage and strain [19].

To address these issues, we have developed a multiscale model that incorporates spatial heterogeneity and links the microscale failure of discrete collagen fibers to the macroscale material response of the tissue. We have initiated our development of a failure theory for soft tissues by examining failure mechanisms in a simpler system that shares some of the properties of native tissues—a reconstituted collagen gel. This model system has been used previously to understand multiscale mechanical interactions and to validate model predictions [20,21]. In the current work, we apply a multiscale scheme to the question of mechanical damage and failure in reconstituted type I collagen gels. We have developed a multiscale model for damage that links the microscale failure of discrete collagen fibers to the macroscale material response of a collagen gel. First, we fitted the model to a series of uniaxial strain-to-failure experiments using a dogbone-shaped sample geometry. Next, we tested the model against an alternative geometry that varied by design—a notched dogbone in uniaxial extension—and gauged its ability in predicting experimental forces, strains, and fiber alignment. In both portions of the study, we use the same collagen source stock for our gels, reconstituted to a specific protein density using the same protocol.

2 Materials and Methods

2.1 Multiscale Model. In our multiscale mechanical model (Fig. 1), representative volume elements (RVEs) comprised of discrete fiber networks determine the mechanical properties of a finite

[1]Corresponding author.

Contributed by the Bioengineering Division of ASME for publication in the JOURNAL OF BIOMECHANICAL ENGINEERING. Manuscript received January 31, 2012; final manuscript received June 9, 2012; accepted manuscript posted July 6, 2012; published online August 27, 2012. Assoc. Editor: Mohammad Mofrad.

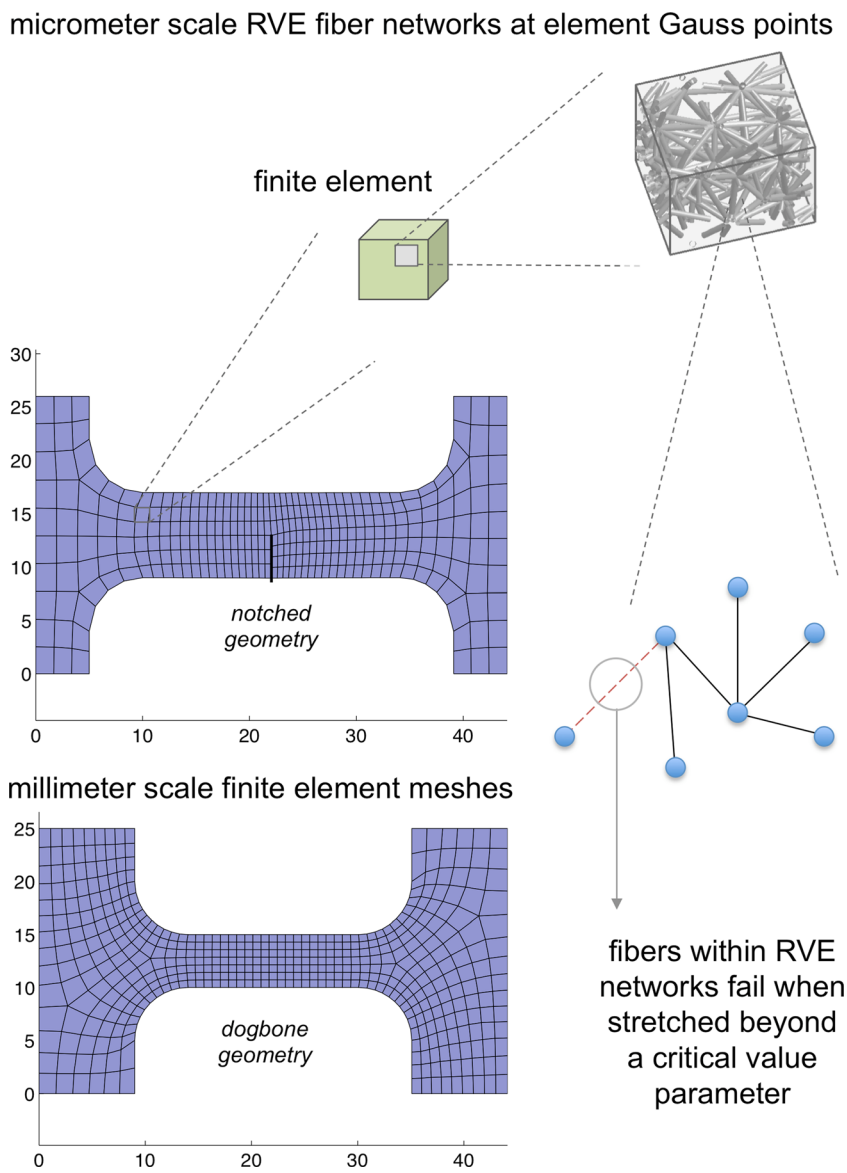

Fig. 1 Overview of the damage model used in the multiscale simulations. The dogbone domain, which exists on the scale of millimeters, is represented with a 3D finite-element mesh. Within each hexahedral element are eight microscopic fiber networks (RVEs) centered at the Gauss points that govern the stress-strain response of the element. As the FE domain stretches, interconnected fibers in the networks stretch and reorganize to satisfy force equilibrium. Fibers that exceed the critical fiber stretch ratio are effectively removed by reducing their modulus by 10 orders of magnitude.

element (FE) continuum at each of its Gauss points (with eight Gauss points assigned to each element using tri-linear basis functions). Typically, RVEs are on the scale of 10–20 μm, whereas the FE domain spans several centimeters. A unique, randomly generated RVE network was assigned to each element in the model. This model has been successfully used to simulate a range of materials [20,22,23]. The method by which macroscale strain is coupled to microscale stress within the model has been described previously [22]. Briefly, macroscale deformations are mapped to deformations of microscale RVE boundaries. The RVE network rearranges and stretches in response to the boundary deformation, generating a volume-averaged stress at each Gauss point within each finite element. The macroscale deformation that balances stress within the continuum is then determined iteratively.

Several governing equations were used in the model to couple macroscale and microscale displacement, force, and stress. The continuum force balance based on the volume-averaged stress from RVE deformations is given by [22]

$$\sigma_{ij,j} = \frac{1}{V}\oint_{\partial V} (\sigma^L_{ij} - \sigma_{ij}) u_{k,i} n_k dS \tag{1}$$

In this equation, σ is the macroscale averaged Cauchy stress, σ^L is the local microscale stress, V is the RVE volume, n is the normal vector to the RVE boundary, u is the displacement of the RVE boundary, and index notation is employed. The RVE volume-averaged Cauchy stress was calculated via the following equation [22]:

$$\sigma_{ij} = \frac{1}{V}\int_V \sigma^L_{ij} dV = \frac{1}{V}\sum_{bc} x_i f_j \tag{2}$$

In this equation bc is the set of all RVE boundary fiber cross-links, x is the boundary fiber cross-link coordinate, f is a component of the force acting on the boundary fiber cross-link, σ is the macroscale averaged Cauchy stress, σ^L is the local microscale stress, and V is the RVE volume. The collagen density of all experimental samples (1.8 mg/ml) was matched exactly in the multiscale model by using the method outlined in Ref. [23], which allowed for the accurate unitization of the mechanical stress-strain response of RVE networks. All model simulations were run on a 32-core parallel cluster at the Minnesota Supercomputing Institute with wall times between 10 and 12 h.

2.2 Microscale Network Damage. At the microscale, networks consist of assemblages of nodes and fibers within a unit cube. Nodes are freely rotating and freely displaced pivots between fibers. Fibers are nonlinear springs with the force along the axis of stretch governed by the nonlinear constitutive equation,

$$F_f = \frac{E_f A_f}{B}(\exp[B\varepsilon_G] - 1) \quad \text{with} \quad E_f \approx 0 \quad \text{for} \quad \lambda_f > \lambda_{\text{crit}} \quad (3)$$

where F_f is the resultant force along a fiber, E_f is the Young's modulus for a fiber at infinitesimal strain, A_f is the fiber cross-sectional area, ε_G is the fiber Green strain, B is a fitting parameter, λ_f is the fiber stretch, and λ_{crit} is the critical fiber stretch value at which damage is triggered. The constitutive equation was adapted from a previous model by Billiar and Sacks [24] for the prefailure mechanics of a collagenous tissue, and the equation has been previously used successfully in multiscale models to capture the mechanical deformation (from small and large strains) of collagen tissue analogs [20,25]. The cross-sectional area A_f for fibers was calculated based on a diameter of 100 nm as seen recently in the work of Lai et al. [25] who performed scanning electron microscopy on reconstituted type I collagen gels, and this diameter is also on the same scale as previous related studies [20,23]. Networks were created from Delaunay tessellations of a set of random points that were originally created in a 2-unit cube and then clipped from the center to produce a 1-unit cube in order to avoid edge effects. Networks had a mean of 456 fibers with a standard deviation of 48 fibers. The chosen number of fibers per RVE network is on the same scale as previous studies using our multiscale model that successfully captured the mechanics of similar collagen gel tissue analogs [20,23]. The chosen topology of networks (as constructed from Delaunay triangulations) was previously compared to alternative topologies of lower nodal degree [26] in uniaxial strain to failure dogbone simulations, and the chosen topology was found to be the best match for experimental outcomes. The model and experimental fiber alignment was initially isotropic in the undeformed configuration (confirmed via polarized light microscopy and then input into the model using isotropic RVE networks) for all simulations considered. Collagen fiber alignment changes can be compared relative to this initial starting point for both model and experiment. Since each macroscale element contains a unique fiber network at each of its eight Gauss points (and simulation FE meshes consisted of several hundred elements), the physics of approximately 1 to 2×10^6 discrete microscale fibers were tracked in each simulation run necessitating the use of supercomputing resources. The small-strain modulus E_f of a fiber within the network was reduced by 10 orders of magnitude (to achieve a near-zero mechanical contribution) if the fiber exceeded a critical stretch value λ_{crit}. This method of implementing damage effectively removed the mechanical contributions of the failed fiber within the network but preserved network topology. This failure model could potentially represent the failure of a fiber or of a fiber-to-fiber cross-link. Fibers were damaged at the end of each macroscale displacement step of 0.10 mm, selected as the minimum displacement step necessary to produce convergent simulation results via trial and error. Fibers are allowed to stretch and rotate in each microscale network within the model (allowing for material reorientation and rearrangement) at each displacement step within the multiscale simulation. All intact fibers in each microscale network are load bearing (not only fibers that span the RVE), and all intact fibers play some role in contributing toward the single volume averaged stress calculated for each RVE in the model. However, fibers are connected to one another only through their original nodal linkages (topology is preserved) within each RVE network, and fibers do not form new linkages during the course of the simulation but rather pass through one another, limiting the manner in which fibers redistribute and interact in the model.

2.3 Collagen Gels. Type I collagen gels were reconstituted from a stock solution of 2.2 mg/ml acid solubilized type I bovine collagen (Organogenesis, Canton, MA) with a final concentration of 1.8 mg/ml using a similar protocol described previously [21]. A solution containing 1 M HEPES (Sigma, St. Louis, MO), 1 M NaOH (Sigma, St. Louis MO) and 10X MEM (Mediatech, Manassas, VA) was used to reconstitute the gels. Gels were cast into molds of two different geometries—dogbone and notched (Fig. 1) each with distinct dimensions—and incubated at 37 °C for approximately 14 h prior to testing. Natural fiber scouring pad strips (3 M, St. Paul, MN) were used as sample anchors in each mold (the gels infiltrate the anchors at casting) and were inserted into molds prior to the addition of the reconstituted gels to facilitate gripping for uniaxial extension. Spring-loaded sandpaper grips were then used to attach the anchors directly to the testing apparatus, alleviating the need to make contact with or apply direct forces to the actual collagen gel sample.

2.4 Mechanical Failure Experiments and Simulations. A series of uniaxial stretch-to-failure experiments were conducted. The gels were tested in two different geometries: dogbone ($n = 5$) and notched ($n = 5$). Experiments were conducted on a low-force planar mechanical tester (Instron, Norwood, MA) in the University of Minnesota Tissue Mechanics Lab. Gels were tested to failure using a chosen grip displacement rate of 0.05 mm/s to elicit a quasi-static force-strain response from samples. The mechanical tester was operated under displacement control at all times. A digital video camera fitted with a 105 mm macro lens (Canon USA, Lake Success, NY) was used to image a selected sample of the notched geometry (speckled with Verhoeff's stain) for optical strain tracking via a custom digital image correlation method previously described in Ref. [27]. Briefly, the strain tracking method relied on the analysis of a series of still images captured from the filmed experiment using a custom code that applied an iterative Newton-Raphson method for pixel displacements based on the work of Ref. [28]. The collagen fiber alignment in a selected notched geometry sample was also imaged during experiments using quantitative polarized light microscopy [21,29,30]. Experimental fiber alignment was quantified using a custom code that analyzed sample images generated using a specialized optical train consisting of a series of polarized light filters [29]. Two separate samples were chosen for either strain analysis or for fiber alignment since we are unable to simultaneously capture both material parameters with our experimental methods. The grip forces and displacements for the dogbone geometry were used to fit key parameters (E_f, the fiber small-strain modulus, B, a nonlinear fitting parameter, and λ_{crit}, the critical fiber stretch for damage) within our static (time-independent) multiscale damage model. Parameters were fit in series by first fitting the macroscopic failure stretch via the critical fiber stretch parameter, next the fiber modulus was fit, and then last, the fiber nonlinear fitting term was fit via a trial and error approach to minimize computational resources expended. The same parameter values were then used to simulate the notched test for comparison against the experimental findings. Several notched test simulations were run ($n = 3$), each using a unique set of RVE fiber networks and with the same key parameters fit from the dogbone geometry. All fibers within the model

were assigned the same material parameters. However, since the network assigned to each element in the model was randomly generated and unique, the effective material properties compared across all elements included some variance.

3 Results

3.1 Dogbone Experiment and Model Fit. Five dogbone samples were loaded to failure, each demonstrating some yielding before failure (Fig. 2). Model parameters (critical fiber failure stretch $\lambda_{crit} = 1.42$, unitless nonlinear fitting parameter $B = 0.25$, and small-strain fiber modulus $E_f = 7.4$ MPa) were determined so that the model peak force and strain at peak force were coincident with the experiment. Using these parameters, the model matched the loading response within the 95% confidence interval for grip force over the entire sample stretch range (Fig. 2), although the model did not demonstrate yielding, and the grip force was generally slightly lower than the mean values observed experimentally. By design, material failure and the bulk of the deformation occurred in the gauge region, defined as the interior region of the dogbone sample consisting of the area encompassed by the two parallel edges within its center. At peak force, the model stretch between the grips was 1.29 as compared with a maximum single element stretch of 1.61. Elements in the flared regions near the grips experienced little stretch in comparison.

A small population of adjoining elements within the gauge region was responsible for the loss of mechanical integrity within the sample (Fig. 2). A specific region of localized elements (which laterally spanned the sample in the center gauge region along two bands of contiguous elements transverse to the direction of loading) experienced the greatest loss of fibers and incurred the greatest element stretches (Fig. 3). The rapid stretch in this region allowed for the retraction of sample regions largely populated by unfailed fiber networks as catastrophic damage ensued. For all of our current and previous dogbone failure simulations, these regions [26] have arisen and expanded within the gauge region of the sample. Fiber networks within these elements lost percolation (Fig. 4) (i.e., there was no connected fiber path across network

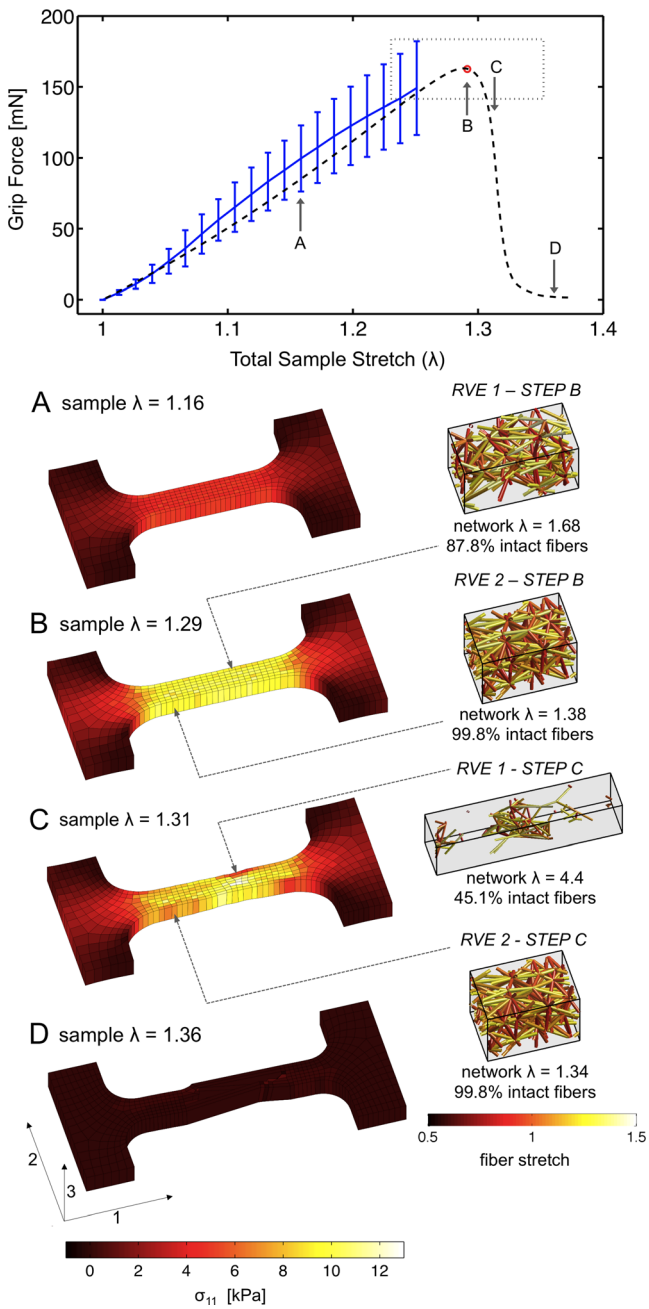

Fig. 2 Dogbone sample: comparison of the grip force against the total sample stretch (λ) for the experiment (solid line ends at first sample failure) and model (dashed line). Error bars represent the 95% confidence interval for the experimental mean (n = 5). The quadrant defined by the dotted lines represents the 95% confidence interval for the peak experimental force and the 95% confidence interval for the experimental strain at peak force. The center of the quadrant is marked with a red circle. The macroscopic stress in the model for select points (*A–D*) along the graph is depicted. Two fiber networks illustrating regional differences in the failure mechanics are also shown and shaded to indicate fiber stretch.

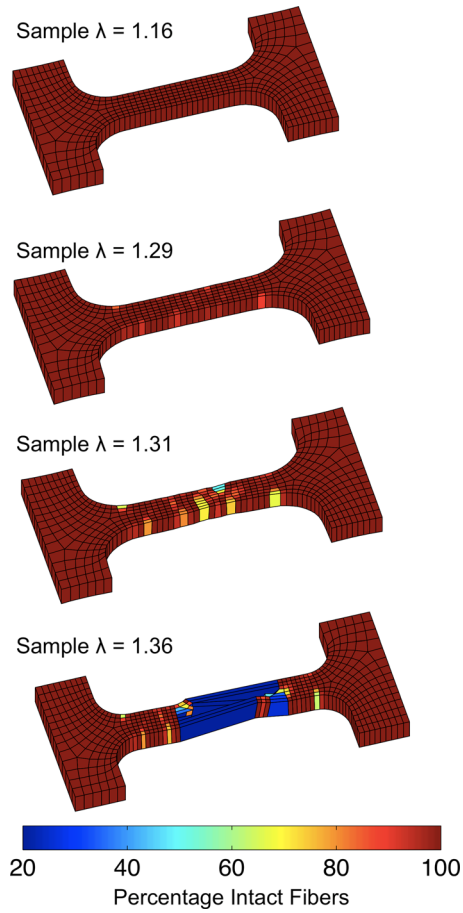

Fig. 3 Percentage of intact fibers per element varies at different grip-to-grip sample stretches (λ) for the model dogbone geometry. Percentage of intact fibers were averaged over all RVE networks within each element.

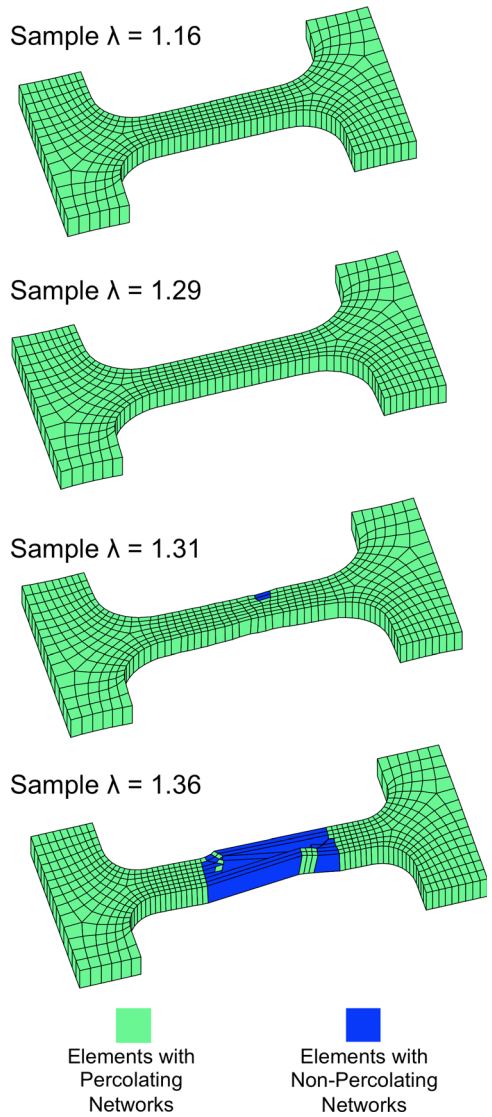

Fig. 4 Elements with nonpercolating networks frame areas of damage for the modeled sample at different grip-to-grip stretches (λ) for the dogbone geometry. A percolating RVE was defined as a network that contained a connected fiber segment that spanned both RVE faces normal to the axis of loading.

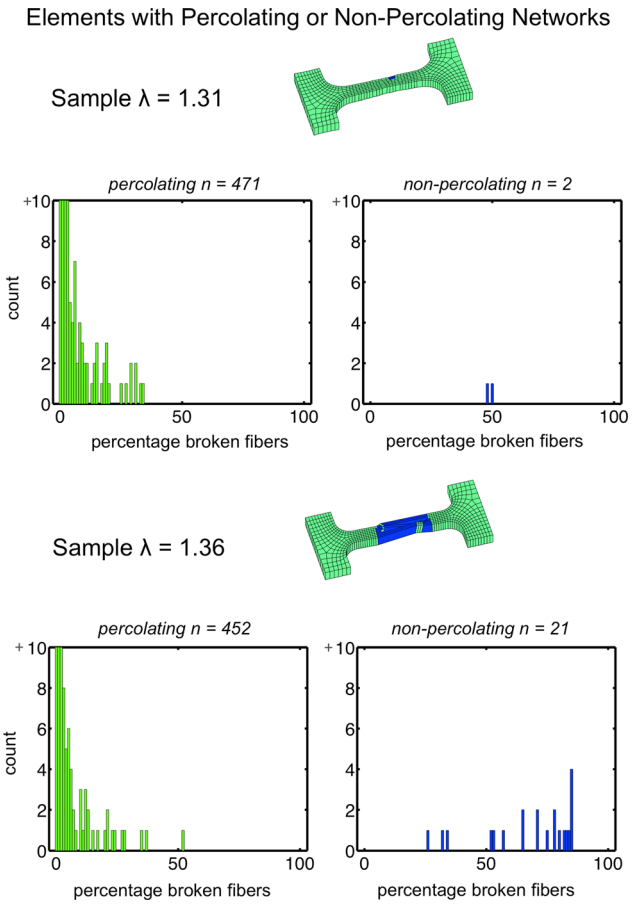

Fig. 5 Comparison of broken fiber percentages in elements with and without percolating RVE networks at different grip-to-grip stretches (λ) for the dogbone geometry

faces) along the axis of stretch and experienced a maximum of 85.4% fiber failure at the end of the simulation as compared with a mean of 4.36% across all elements (Fig. 5). The majority of elements, 61.5%, experienced no fiber failure during the simulation. Fibers that were left intact in nonpercolating networks were found in unconnected clusters attached to RVE network faces or were contained in isolated fiber islands. Fibers in nonpercolating networks were analyzed following catastrophic failure in the dogbone sample (at a grip-to-grip macroscopic sample stretch of 1.36) and fibers were distributed according to the mean fiber orientation tensor Ω (as defined in Ref. [23]) with diagonal terms $[\Omega_{11}\ \Omega_{22}\ \Omega_{33}]$ equal to [0.35 0.32 0.33], indicating that remaining intact fibers were not simply arrayed orthogonal to the axis of extension and likely retracted upon the failure of the majority of fibers within the network. For context, all networks were initially isotropic on average with a mean fiber orientation tensor Ω containing diagonal terms $[\Omega_{11}\ \Omega_{22}\ \Omega_{33}]$ equal to [0.33 0.33 0.33] throughout the system before any strains were applied. It is important to note that while we have plotted distributions of intact fibers and network percolation within the model at different simulation points, we are unable to investigate the actual microscale deformation of the experimental collagen fiber network with our current experimental setup to compare against simulated results.

In the simulation, the single element with the largest Cauchy σ_{11} stress at peak grip force (loaded in axis 1) was not contained within the element set that experienced the greatest fiber failure and that subsequently lost mechanical integrity over the sample stretch (Fig. 6). Instead, elements that experienced the greatest strain along the axis of loading at peak grip force (and after) were elements where macroscale failure initiated within the gauge region of the sample. Elements coincident with peak strain during the simulation also experienced the greatest loss of collagen fibers at the microscale. In all of our previous multiscale simulations of failure in dogbone samples [26], failure has taken place in the gauge region of the sample geometry regardless of networks selected for the model. In the present study, we have not considered the role of stochasticity in the dogbone simulation case. Rather, the role of independent simulations with unique networks (n = 3) was considered in the case of the notch validation simulations. A bimodal distribution of element stretches along the axis of loading arose near the moment of peak grip force (as one population of elements had largely failed while another population of elements was left largely intact) as particular elements already began to experience stretches that were 35%–40% greater than the mean element stretch (Fig. 7).

Since RVE networks were generated randomly and were on average isotropic but included some variance in their mechanical stiffness, we calculated the tangent modulus of all networks used in the simulation at large deformations (using a uniaxial stretch of 1.4 for each network) to see if this statistic played a role in macroscale failure. Elements in the gauge region containing networks with the largest tangent moduli were, unsurprisingly, not coincident with

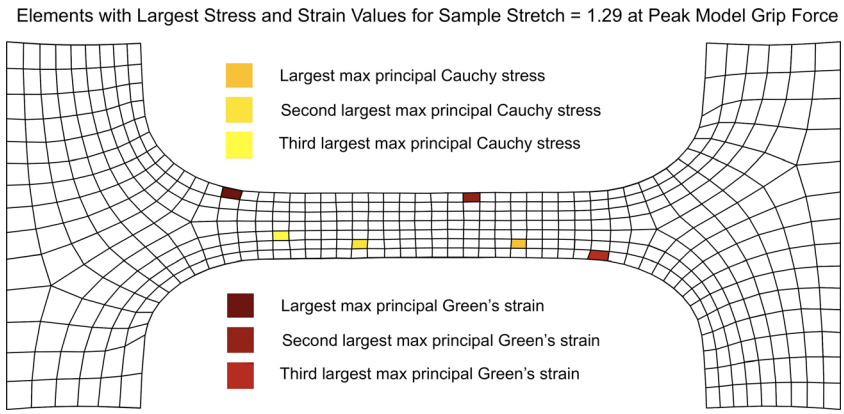

Fig. 6 The peak max principal Cauchy stress and the peak max principal Green strain for the dogbone geometry plotted over the deformed finite element mesh at the point of greatest grip force in the model

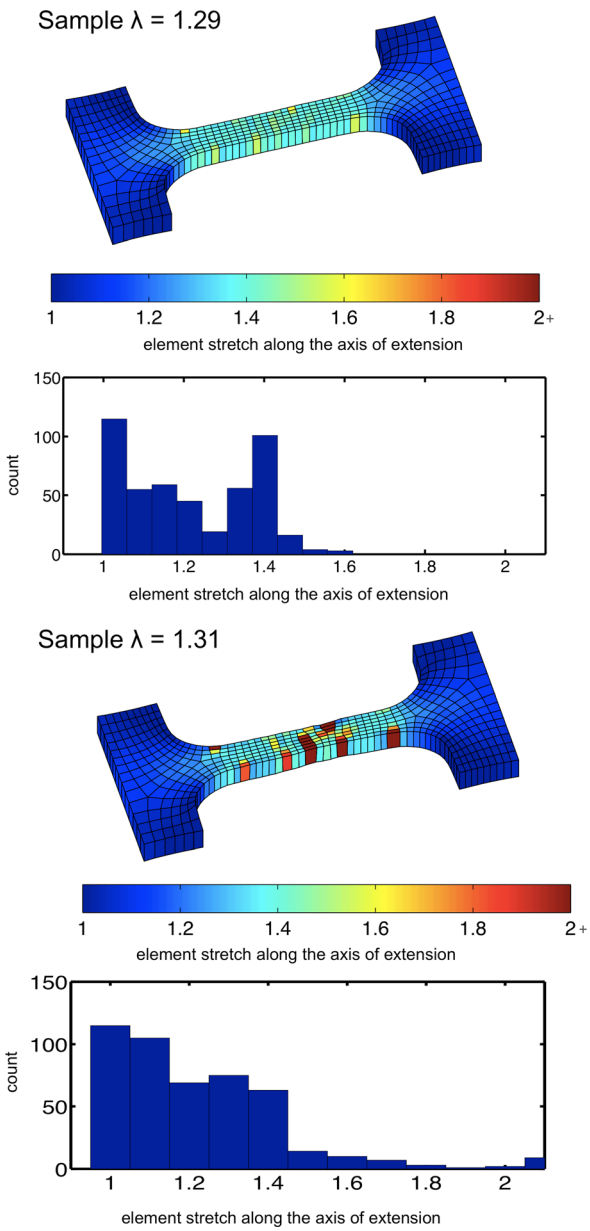

Fig. 7 Element stretch (along the axis of extension) plotted over the deformed mesh for the model dogbone geometry. The element stretch is also represented via corresponding histograms at a given sample stretch (λ) for the dogbone geometry.

regions of greatest strain and greatest fiber failure in the model. However, elements which contained networks with the smallest tangent moduli values did not experience the greatest strains or the greatest fiber failure in the model, suggesting that while tangent moduli plays some role in framing damage within the model, there is an interplay between overall macroscale kinematics, network stiffness, and network variation that leads to catastrophic failure within the multiscale system.

3.2 Notched Dogbone Experiment and Model Predictions. For the failure of samples in the notched geometry simulated with fitted parameters from the dogbone geometry, we found that the predicted forces fell within the 95% confidence interval for all grip forces above a sample stretch of 1.08 (Fig. 8). In this case, the predicted grip forces were generally higher than those of the experiment, which featured a shallower toe region as compared to the dogbone experiment. The mean peak simulated force, and the mean stretch at peak force fell within 15% of the experimental values. Failure in the simulated notch case, similar to failure experiments with notched collagen gels, was characterized by a propagation of the stress concentrator through the axis perpendicular to the direction of stretch.

At the end of the notch simulation, only 10.0% of elements had experienced fiber failure as compared to 38.5% for the dogbone case. Elements experiencing fiber failure were concentrated along a path parallel to the crack tip (Fig. 9). The maximum fiber failure percentage for these elements was 89.8%. At the mean peak simulated force, the grip sample stretch along the axis of extension was 1.17 and was compared to an average stretch of 1.30 in the central region spanning the notch, though the maximum element stretch was 2.08 near the notch tip.

Percolation in RVE networks across the axis of stretch was lost for elements for the dogbone and notched case only after the peak force for these simulations was reached. 89% of elements that lost percolation along this axis had lost greater than 45% of their fibers during the simulation (Figs. 10 and 11). Only 5 of 312 elements for the notch geometry lost percolation while 21 of 473 elements lost percolation in the dogbone geometry. It is important to note that in both the notch and dogbone simulations all RVE networks were similarly generated and began as initially percolating and isotropic, with the notch modeled in the macroscale FE mesh of the simulation, not through any microscale RVE network alterations. The loss of percolation in elements was characterized by a sharp drop in the grip force for each simulation, leading to a catastrophic loss of mechanical integrity.

Simulated outcomes for the strain field and fiber alignment at peak grip force were also compared to the experimental case (as measured by digital image correlation) for the notched geometry (Fig. 12). Qualitatively, areas of greatest strain in the sample

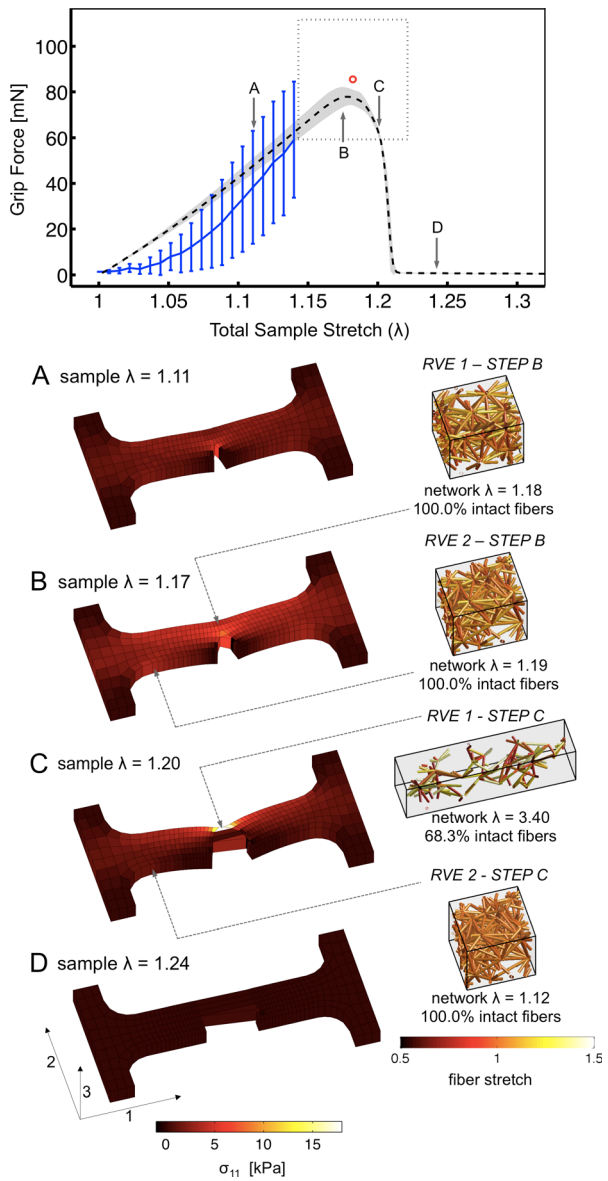

Fig. 8 Notched sample: comparison of the grip force against the total sample stretch (λ) for the experiment (solid line ends at first sample failure) and model prediction (dashed line is the mean result and gray area represents the 95% confidence interval for n = 3 independent simulations). Error bars represent the 95% confidence interval for the experimental mean (n = 5). The quadrant defined by the dotted lines represents the 95% confidence interval for the peak experimental force and the 95% confidence interval for the experimental strain at peak force. The center of the quadrant is marked with a red circle. The macroscopic stress in the model for select points (*A–D*) along the graph is depicted. Two fiber networks illustrating regional differences in the failure mechanics are also shown and shaded to indicate fiber stretch.

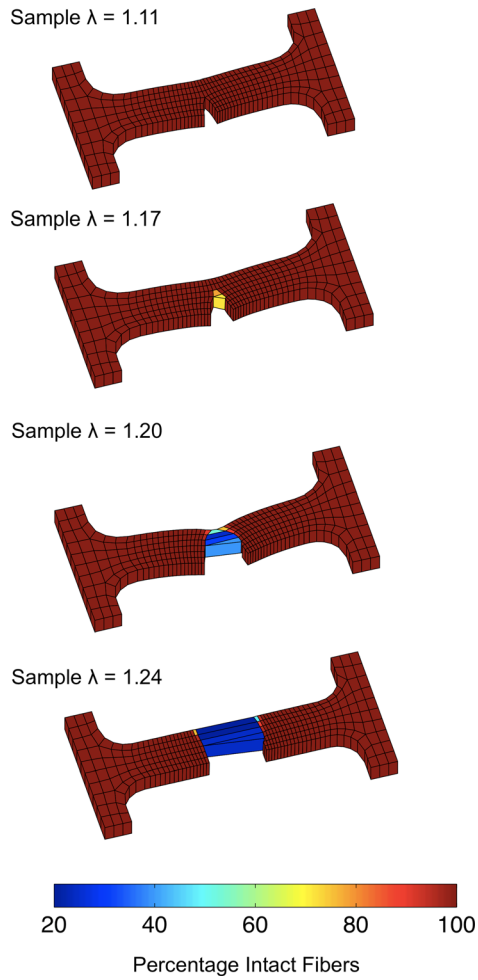

Fig. 9 Percentage of intact fibers per element varies at different grip-to-grip sample stretches (λ) for the notched geometry model. Percentage of intact fibers were averaged over all RVE networks within each element.

corresponded between simulation and experiment, centering at the notch tip. Discounting elements whose networks contained a majority of failed fibers, the peak Green strain components in the direction of extension near the notch tip fell within 0.3 and 0.5 for the model and experimental case. Fibers became highly aligned in the experimental case (as measured by quantitative polarized light microscopy) along the axis of stretch over the unnotched region of the sample. Fibers were left relatively unaligned in regions along the axis of stretch through the notched region of the experimental sample. This trend was also seen in the simulated case, but there was greater realignment of fibers along the edges of the notch perpendicular to the axis of stretch. There was also less variation in alignment along the unnotched portion of the experimental sample as compared with the simulated result.

4 Discussion

The model may be a useful tool in predicting the macroscale failure conditions for engineered tissue analogs in complex geometries based either on fitted values from simple experimental geometries or from experimentally derived microstructural values for fiber failure. For our collagen gel model, we were able to demonstrate that a fiber-based rule (at the micrometer scale) for discrete failure could strongly shape the macroscale failure response of the gel (at the millimeter level). The agreement between the model and the experiments demonstrates the ability to predict tissue-level events based on a microstructural model. The systems studied were relatively simple in that the samples were of uniform collagen density and were initially isotropic. The extension to more complex geometries and architectures, however, as arise in native tissues [19,31] and bioengineered tissues [32,33], would be difficult to model at the tissue scale without an underlying structural description. A major advance of the current work is the potential to accommodate regional structural variation without requiring a change in the failure criteria.

In order for us to realize that potential, however, a better understanding of fiber-level failure mechanisms is needed. One might well argue that we have replaced the intractable problem of

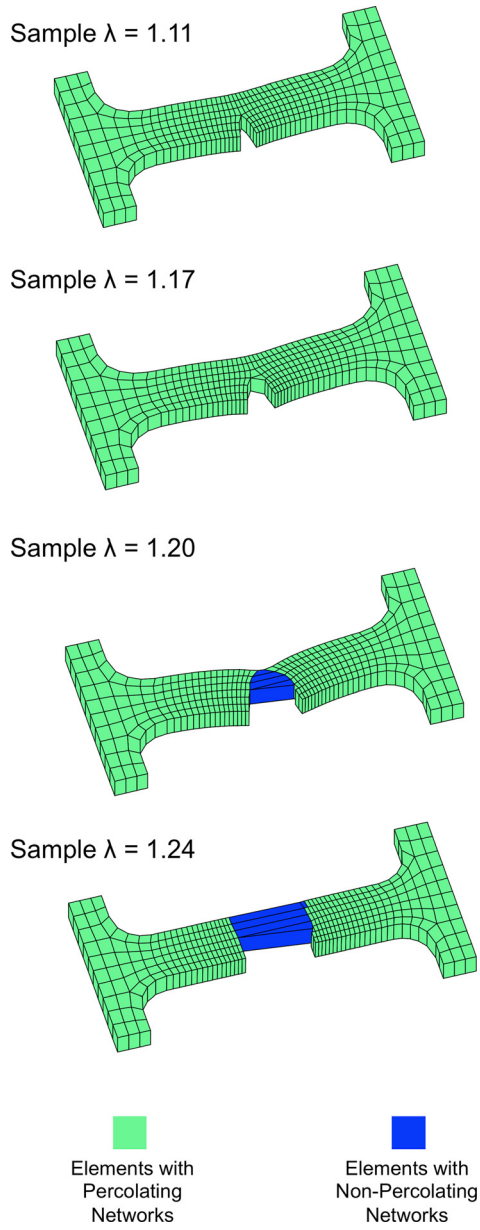

Fig. 10 Elements with nonpercolating networks frame areas of damage for the modeled sample at different grip-to-grip stretches (λ) for the notched geometry. A percolating RVE was defined as a network that contained a connected fiber segment that spanned both RVE faces normal to the axis of loading.

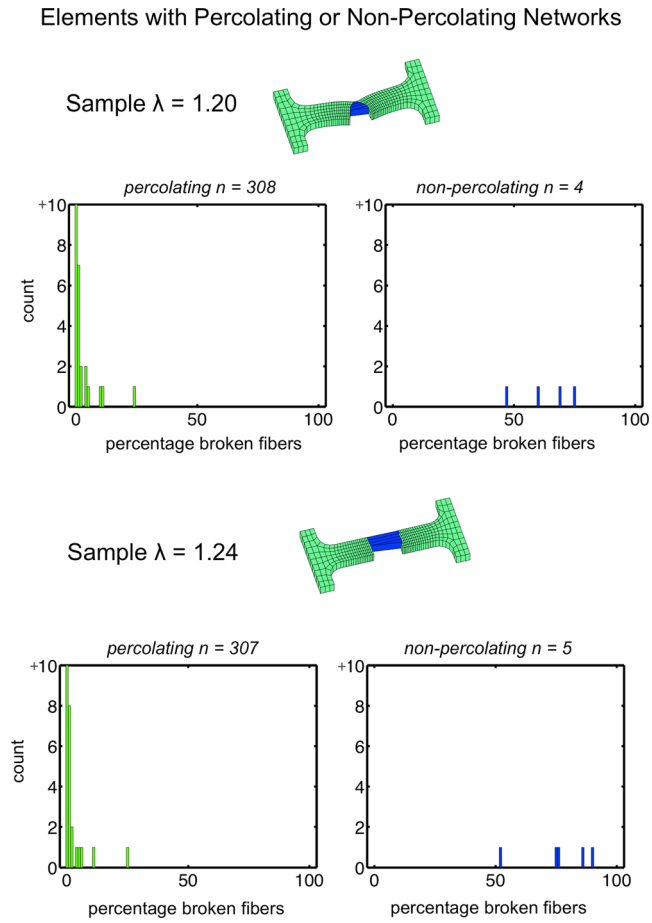

Fig. 11 Comparison of broken fiber percentages in elements with and without percolating RVE networks at different notched model grip-to-grip stretches

modeling failure at the tissue level with the merely difficult problem of modeling it at the fiber level. The current work used the simplest possible failure model—no damage until a critical strain is reached, at which point the fiber fails catastrophically—which is appropriate for a single strain-to-failure experiment as performed here but would not be able to capture a fatigue mechanism in which repeated loading cycles contribute to the failure of the tissue. Advances in single-collagen-fiber mechanical analysis [34] are steadily increasing our understanding of fiber behavior and will be particularly informative on this point. Direct comparisons to previous studies of single-fiber failure in type I collagen (both experimental and simulated) while useful for context, are limited by differences in fiber diameter, intrafibrillar cross-linking, hydration, and collagen source. Shen et al. [34] experimentally strained type I collagen fibrils (native to sea cucumbers with diameters ranging from 150 to 470 nm) uniaxially and observed a mean yield stretch of 1.21 ± 0.13 with observed fiber failure occurring over a broader range with select fibers stretching well beyond this range without failure. Buehler [35] has predicted, using purely atomistic modeling, tropocollagen molecule (subfibrillar) failure stretches between 1.4 and 1.6 via reactive force modeling. Pins et al. [33] experimentally found failure stretches for uncrosslinked reconstituted type I collagen fibers ranging from approximately 1.2 to 1.7 for much larger hydrated diameters falling between 120 and 330 μm. Our chosen fiber failure parameter of 1.42 for all of our simulations falls within the range of these previous findings for fiber-level or sub-fiber-level failure stretch values. However, since fiber failure in our model may represent either the mechanical failure of fibers or potentially the failure of fiber-to-fiber linkages, direct comparisons are elusive. The small variance in our simulated outcome for the notched geometry (measured via the simulated grip force or sample stretch) relative to the experiment suggests that we may need to consider the possibility of stepped fiber failure or that we need to include greater variability in our model networks (perhaps by utilizing fiber diameter distributions) or by employing probabilistic rules for fiber failure. Furthermore, better understanding of network structure, and of what parameters are needed to characterize the network structure and to develop realistic network geometries [36], is also necessary to strengthen the model.

There is a growing body of work exploring the role of network structure in damage. Important two-dimensional examples include the work of Bates et al. on elastic fiber networks in the lung [37,38] and Keten et al. [8] on protein networks, all of which used structured networks with random variations in fiber properties to capture variability. Black et al. [39] have successfully used a zipper network model to add context to their experimental findings

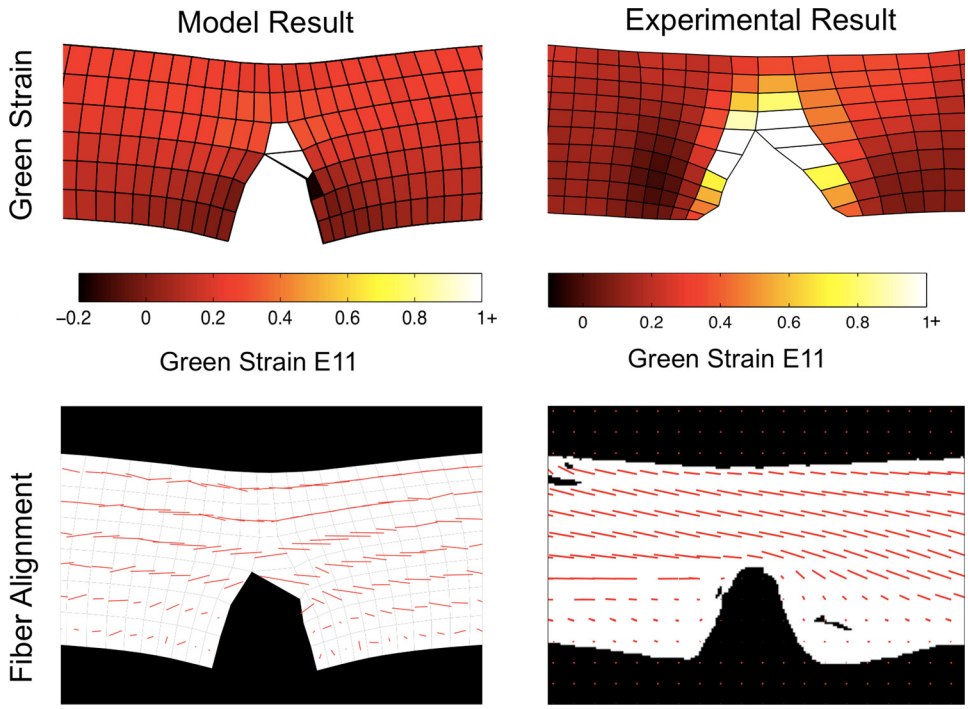

Fig. 12 Comparison of the model and experiment for the Green strain and collagen fiber alignment (alignment vectors normalized by maximum strength of alignment) at the point of peak grip force for the deformed notch geometry for two independent experimental samples

on the failure of engineered extracellular matrices. However, none of these studies, nor any other to our knowledge, have linked subfailure microscale damage to the macroscale failure properties of tissue analogs as we have demonstrated in the present study. The analysis of the loss of percolation in the three-dimensional Delaunay networks employed in our model also adds to existing work on quantifying percolation thresholds for various instances of Delaunay triangulation lattices such as the recent study by Becker and Ziff [40] that numerically calculated an edge percolation threshold between 0.33 and 0.35 for two-dimensional random Delaunay lattices. In our three-dimensional networks, we find that when a fraction of nearly 0.55 fibers (edges) are connected in mechanical networks extended along a single axis, in most instances, percolation is preserved along the same axis.

Finally, we note that most tissues involve multiple fiber networks (e.g., fibrin and collagen) and/or a significant quantity of nonfibrillar macromolecules (e.g., proteoglycans), which could be extremely important in understanding the failure and subfailure behavior of a tissue. Gross tissue failure obviously must include failure of all components and might reasonably be expected to include (and, in many cases, be dominated by) the failure of a collagen network, but subfailure damage may well involve other components in nonobvious ways.

Acknowledgment

This work was supported by the National Institutes of Health (R01-EB005813) and by a National Science Foundation Graduate Fellowship in Science and Engineering. Computational resources were provided by the Minnesota Supercomputing Institute.

References

[1] Quinn, K. P., and Winkelstein, B. A., 2011, "Detection of Altered Collagen Fiber Alignment in the Cervical Facet Capsule After Whiplash-Like Joint Retraction," Ann. Biomed. Eng., **39**(8), pp. 2163–2173.
[2] Phillippi, J. A., Pasta, S., and Vorp, D. A., 2011, "Biomechanics and Pathobiology of Aortic Aneurysms," Biomech. Mechanobiol. Aneurysms, **7**, pp. 67–118.
[3] Hurschler, C., Loitz-Ramage, B., and Vanderby, R., Jr., 1997, "A Structurally Based Stress-Stretch Relationship for Tendon and Ligament," J. Biomech. Eng., **119**(4), pp. 392–400.
[4] Wren, T. A., Yerby, S. A., Beaupré, G. S., and Carter, D. R., 2001, "Mechanical Properties of the Human Achilles Tendon," Clin. Biomech. (Bristol, Avon), **16**(3), pp. 245–251.
[5] Liao, H., and Belkoff, S. M., 1999, "A Failure Model for Ligaments," J. Biomech., **32**(2), pp. 183–188.
[6] De Vita, R., and Slaughter, W. S., 2007, "A Constitutive Law for the Failure Behavior of Medial Collateral Ligaments," Biomech. Model. Mechanobiol., **6**(3), pp. 189–197.
[7] Ritter, M. C., Jesudason, R., Majumdar, A., Stamenović, D., Buczek-Thomas, J. A., Stone, P. J., Nugent, M. A., Suki, B., 2009, "A Zipper Network Model of the Failure Mechanics of Extracellular Matrices," Proc. Natl. Acad. Sci. U.S.A., **106**(4), pp. 1081–1086.
[8] Keten, S., Bertaud, J., Sen, D., Xu, Z., Ackbarow, T., and Buehler, M. J., 2010, "Multiscale Modeling of Biological Protein Materials–Deformation and Failure," Trends Comput. Nanomech., **9**, pp. 473–533.
[9] Ackbarow, T., Sen, D., Thaulow, C., and Buehler, M. J., 2009, "Alpha-Helical Protein Networks are Self-Protective and Flaw-Tolerant," PLoS ONE, **4**(6), p. e6015.
[10] Sastry, A., Cheng, X., and Wang, C., 1998, "Mechanics of Stochastic Fibrous Networks," J. Thermoplast. Compos. Mater., **3**(11), pp. 288–296.
[11] Wang, C. W., and Sastry, A. M., 2000, "Structure, Mechanics and Failure of Stochastic Fibrous Networks: Part II—Network Simulations and Application," J. Eng. Mater. Technol., **122**, pp. 460–469.
[12] Zohdi, T., 2007, "A Computational Framework for Network Modeling of Fibrous Biological Tissue Deformation and Rupture," Comput. Methods Appl. Mech. Eng., **196**(31), pp. 2972–2980.
[13] Ernst, G., Vogler, M., Hühne, C., and Rolfes, R., 2010, "Multiscale Progressive Failure Analysis of Textile Composites," Compos. Sci. Technol., **70**(1), pp. 61–72.
[14] Gilbert, T. W., Sacks, M. S., Grashow, J. S., Savio, L. Y. W., Badylak, S. F., and Chancellor, M. B., 2006, "Fiber Kinematics of Small Intestinal Submucosa Under Biaxial and Uniaxial Stretch," J. Biomech. Eng., **128**, pp. 890–898.
[15] Billiar, K. L., and Sacks, M. S., 1997, "A Method to Quantify the Fiber Kinematics of Planar Tissues Under Biaxial Stretch," J. Biomech., **30**(7), pp. 753–756.
[16] Lake, S. P., Miller, K. S., Elliott, D. M., and Soslowsky, L. J., 2009, "Effect of Fiber Distribution and Realignment on the Nonlinear and Inhomogeneous Mechanical Properties of Human Supraspinatus Tendon Under Longitudinal Tensile Loading," J. Orthop. Res., **27**(12), pp. 1596–1602.
[17] Padala, M., Sacks, M. S., Liou, S. W., Balachandran, K., He, Z., and Yoganathan, A. P., 2010, "Mechanics of the Mitral Valve Strut Chordae Insertion Region," J. Biomech. Eng., **132**, p. 081004.
[18] Moger, C., Arkill, K., Barrett, R., Bleuet, P., Ellis, R., Green, E., and Winlove, C., 2009, "Cartilage Collagen Matrix Reorientation and Displacement in Response to Surface Loading," J. Biomech. Eng., **131**, p. 031008.

[19] Quinn, K. P., and Winkelstein, B. A., 2008, "Altered Collagen Fiber Kinematics Define the Onset of Localized Ligament Damage During Loading," J. Appl. Phys., **105**(6), pp. 1881–1888.
[20] Sander, E. A., Stylianopoulos, T., Tranquillo, R. T., and Barocas, V. H., 2009, "Image-Based Multiscale Modeling Predicts Tissue-Level and Network-Level Fiber Reorganization in Stretched Cell-Compacted Collagen Gels," Proc. Natl. Acad. Sci. U.S.A., **106**(42), pp. 17675–17680.
[21] Sander, E. A., Stylianopoulos, T., Tranquillo, R. T., and Barocas, V. H., 2009, "Image-Based Biomechanics of Collagen-Based Tissue Equivalents: Multiscale Models Compared to Fiber Alignment Predicted by Polarimetric Imaging," IEEE Eng. Med. Biol. Mag., **28**(3), pp. 10–18.
[22] Chandran, P. L., and Barocas, V. H., 2007, "Deterministic Material-Based Averaging Theory Model of Collagen Gel Micromechanics," J. Biomech. Eng., **129**, pp. 137–147.
[23] Stylianopoulos, T., and Barocas, V. H., 2007, "Volume-Averaging Theory for the Study of the Mechanics of Collagen Networks," Comput. Methods Appl. Mech. Eng., **196**(31-32), pp. 2981–2990.
[24] Billiar, K. L., and Sacks, M. S., 2000, "Biaxial Mechanical Properties of the Native and Glutaraldehyde-Treated Aortic Valve Cusp: Part II—A Structural Constitutive Model," J. Biomech. Eng., **122**, pp. 327–335.
[25] Lai, V. K., Lake, S. P., Frey, C. R., Tranquillo, R. T., and Barocas, V. H., 2012, "Mechanical Behavior of Collagen-Fibrin Co-Gels Reflects Transition From Series to Parallel Interactions With Increasing Collagen Content," J. Biomech. Eng., **134**, p. 011004.
[26] Sander, E. A., Hadi, M. F., and Barocas, V. H., 2011, "Multiscale Mechanical Models for Understanding Microstructural Damage in Fibrous Tissues," Proceedings of the ASME 2011 Summer Bioengineering Conference, Farmington, PA, Paper No. SBC2011-53781.
[27] Raghupathy, R., Witzenburg, C., Lake, S. P., Sander, E. A., and Barocas, V. H., 2011, "Identification of Regional Mechanical Anisotropy in Soft Tissue Analogs," J. Biomech. Eng., **133**, p. 091011.
[28] Pan, B., Asundi, A., Xie, H., and Gao, J., 2009, "Digital Image Correlation Using Iterative Least Squares and Pointwise Least Squares for Displacement Field and Strain Field Measurements," Opt. Lasers Eng., **47**(7-8), pp. 865–874.
[29] Tower, T. T., Neidert, M. R., and Tranquillo, R. T., 2002, "Fiber Alignment Imaging During Mechanical Testing of Soft Tissues," Ann. Biomed. Eng., **30**(10), pp. 1221–1233.
[30] Sander, E., and Barocas, V., 2009, "Comparison of 2D Fiber Network Orientation Measurement Methods," J. Biomed. Mater. Res. Part A, **88**(2), pp. 322–331.
[31] Sacks, M. S., Schoen, F. J., and Mayer, J. E., Jr., 2009, "Bioengineering Challenges for Heart Valve Tissue Engineering," Annu. Rev. Biomed. Eng., **11**, pp. 289–313.
[32] Robinson, P. S., and Tranquillo, R. T., 2009, "Planar Biaxial Behavior of Fibrin-Based Tissue-Engineered Heart Valve Leaflets," Tissue Eng., **15**(10), pp. 2763–2772.
[33] Pins, G. D., Huang, E. K., Christiansen, D. L., and Silver, F. H., 1997, "Effects of Static Axial Strain on the Tensile Properties and Failure Mechanisms of Self-Assembled Collagen Fibers," J. Appl. Polym. Sci., **63**(11), pp. 1429–1440.
[34] Shen, Z. L., Dodge, M. R., Kahn, H., Ballarini, R., and Eppell, S. J., 2008, "Stress-Strain Experiments on Individual Collagen Fibrils," Biophys. J., **95**(8), pp. 3956–3963.
[35] Buehler, M. J., 2006, "Nature Designs Tough Collagen: Explaining the Nanostructure of Collagen Fibrils," Proc. Natl. Acad. Sci. U.S.A., **103**(33), pp. 12285–12290.
[36] Stein, A. M., Vader, D. A., Weitz, D. A., and Sander, L. M., 2008, "The Micromechanics of Three Dimensional Collagen-I Gels," Complexity, **16**(4), pp. 22–28.
[37] Bates, J. H. T., 2007, "A Recruitment Model of Quasi-Linear Power-Law Stress Adaptation in Lung Tissue," Ann. Biomed. Eng., **35**(7), pp. 1165–1174.
[38] Maksym, G. N., Fredberg, J. J., and Bates, J. H. T., 1998, "Force Heterogeneity in a Two-Dimensional Network Model of Lung Tissue Elasticity," J. Appl. Phys., **85**(4), pp. 1223–1229.
[39] Black, L. D., Allen, P. G., Morris, S. M., Stone, P. J., and Suki, B., 2008, "Mechanical and Failure Properties of Extracellular Matrix Sheets as a Function of Structural Protein Composition," Biophys. J., **94**(5), pp. 1916–1929.
[40] Becker, A. M., and Ziff, R. M., 2009, "Percolation Thresholds on Two-Dimensional Voronoi Networks and Delaunay Triangulations," Phys. Rev. E, **80**(4), p. 041101.